Korean J. Chem. Eng., 34(2), 500-510 (2017)
DOI: 10.1007/s11814-016-0284-2

pISSN: 0256-1115
eISSN: 1975-7220

Formation of intermediate band and low recombination rate in ZnO-$BiVO_4$ heterostructured photocatalyst: Investigation based on experimental and theoretical studies

Sonal Singh*, Rishabh Sharma, Girdhar Joshi***,†, and Jitendra Kumar Pandey*,†**

*University of Petroleum and Energy Studies (UPES), VPO Bidholi, PO Prem Nagar, Dehradun 248007, India
**Thin Film Laboratory, Department of Physics, Indian Institute of Technology, New Delhi-110016, India
***Department of Chemistry, Government Post Graduate College, Gopeshwar, Uttarakhand, India
(*Received 14 July 2016 • accepted 11 October 2016*)

Abstract−We present systematic investigations on the relationship between interface formation and enhanced photocatalytic activity of ZnO-$BiVO_4$ nanocomposite based on experimental techniques supported by theoretical calculations. The interaction between ZnO (101) nanosheet and $BiVO_4$ surface at the heterojunction was explored to study the charge transfer and separation mechanism responsible for enhanced photocatalytic response. XPS results and DFT computations mutually validate the reasonable existence of ZnO-$BiVO_4$ interface. The nanocomposite photocatalytic activity, tested for various weight ratios, was found to be highest for ZnO-$BiVO_4$ (1 : 1) under visible-light irradiation. Moreover, the percentage removal of MB was found to be greater than RhB for the same time duration. Steady state and time resolve photoluminescence were employed to understand the carrier lifetime and emissivity. Visible light driven high photoactivity exhibited by ZnO-$BiVO_4$ (1 : 1) was ascribed to the formation of intermediate band and comparatively low recombination rate, which facilitates the separation of electron-hole pairs. Based on the theoretical outcome, we found that valence band maximum was occupied by Bi s orbital and conduction band minimum was occupied by Zn s orbital, which indicates the maximum electron transition from $BiVO_4$ valence band to ZnO conduction band in ZnO-$BiVO_4$ composite. These results demonstrated that heterojunction semiconductors are an effective strategy that can be successfully applied to develop photocatalysts that respond to visible light for organic pollutant degradation.

Keywords: Zinc Oxide, Monoclinic-bismuth Vanadate, Intermediate Band, DFT, Time Resolved PL

INTRODUCTION

Photocatalysis is a rapidly emerging research area with ever growing demand in environment and energy related industries for various applications, including purification and treatment of water [1,2] and air [3-5], degradation of organic pollutants [6,7] and production of renewable fuels [8,9]. Organic pollutants in water such as waste dyes, surfactants and other harmful chemicals from industries are major threats to the environment and mankind. Photocatalysts, in the presence of light, have the ability to produce reactive oxidizing agents [10,11] that degrade the toxic organic materials, and no waste residue is produced during this process [11,12]. Also, the photocatalyst itself does not undergo any chemical reaction and thus can be used repeatedly, resulting in simpler and cost-effective setup [12]. Significant research efforts have been made to come up with new and superior photocatalyst materials, not only in terms of their dye degradation efficiency but for improved photo stability and reaction repeatability. Besides TiO_2 [12-14] and its composites as photo catalytically active materials, a large number of non-TiO_2 based materials (mostly metal oxides) [15-17] have been found to display strong photocatalytic response.

Materials like ZnO, which has high potential for good photocatalysts in UV region [18], has drawbacks owing to its large band gap (which mainly governs the phenomenon of photocatalysis) and thus it is important to tailor its electronic and optical properties (to modify the rate of chemical reaction). Construction of heterojunction by producing an interface between ZnO and another semiconductor material with unequal bandgap is one such effective strategy. ZnO based heterostructures/composites [19-23] such as Au-ZnO, Pt-ZnO, ZnO/Ag/Mn_2O_3, Fe_2O_3/$ZnFe_2O_4$/ZnO, and AuPd/ZnO/RGO with improved electro-optic properties have been found to work well in the visible region of the solar spectrum than pure ZnO. ZnO has an edge over narrow band gap material in terms of its suitable band edge positions which are beneficial for complete splitting of water [24] into hydrogen and hydroxyl ions, but at the same time the latter are more adapted to solar spectrum and thus show improved response to visible spectrum region. Much explored Bismuth Vanadate has a suitable visible-light active narrow bandgap for photocatalysis [25], but simultaneously suffers from inappropriate band edge position for reduction of water; rather, it is suitable only for oxidation of water due to slightly positive conduction band edge than 0 V, making it inefficient for complete redox of water [26,27]. Therefore, composite blends the advantage of both

†To whom correspondence should be addressed.
E-mail: drgirdharjoshi@yahoo.in, gdcsmcri@gmail.com, jkpandey@ddn.upes.ac.in

the materials showing effective utilization of solar spectrum due to the presence of $BiVO_4$ and increased water redox efficiency due to wide band gap of ZnO.

ZnO and $BiVO_4$-based nanocomposites are newly emerging materials in this area and are known to show enhanced photocatalysis as compared to their pristine counterparts. Not much work has been done in this direction, and this provides a large scope to explore this nanocomposite. Theoretical investigations based on potential of heterostructures to tune the electronic properties of the composite are still lacking [28-30].

Motivated by impressive studies on heterostructures of ZnO, we focused on synthesis and investigating the mechanism of interface interaction of charge transfer and separation on photocatalytic activity of ZnO and $BiVO_4$ based nanocomposite. The remarkable increase in photocatalytic activity and reduced band gap (2.94 eV) of ZnO-$BiVO_4$, without the use of any supportive charge transport medium or co-catalyst, is due to the formation of intermediate band at interface, formed during the mechanical milling and annealing [31] process of synthesis. The synthesized nanocomposite samples with different weight ratios were tested on two model contaminants from textile industries; i.e., MB and RhB and showed different degradation efficiency for both the dyes. The probable reason for this difference is discussed in this study. Theoretical calculations further provided a detailed insight of the heterojunction which confirmed the formation of the interface.

EXPERIMENTAL

1. Synthesis of the ZnO-$BiVO_4$ Photocatalysts

All the analytical grade chemicals were purchased from Sigma Aldrich India and were used in experimentation without any further purification. $BiVO_4$ nanoparticles and ZnO nanosheets were synthesized by the hydrothermal route. In detail, 6 mM (2 gms) of $Bi(NO_3)_3{\cdot}5H_2O$ was dissolved in 50 ml of 2.4 molar HNO_3 solution and 6 mM (0.7 gms) NH_4VO_3 was dissolved in another 50 ml of 1.9 molar NaOH solution to form yellow amorphous $BiVO_4$ solution. Similarly, 10 mM (2 gms) of $Zn(O_2CCH_3)_2(H_2O)_2$ was dissolved in 50 ml of DI water and 20 mM (0.78 gms) of NaOH was dissolved in another 50 ml of DI water to form white ZnO solution. Then, 1 and 2 gm of Sodium Dodecyl Benzene Sulphonate (SDBS) was added to both the solutions of $BiVO_4$ and ZnO, respectively, followed by rigorous magnetic stirring for 1 h. The precursor solutions were then poured into separate 100 ml Teflon-lined stainless steel autoclave so that they occupied 80% of the volume of the autoclave. The autoclaves were heated at 200 °C [32] for both the samples for four hours for $BiVO_4$ and six hours for ZnO. After completion of the reaction, the reaction mixture was cooled to room temperature to obtain brilliant yellow $BiVO_4$ and white ZnO precipitate. Precipitates were centrifuged and washed with DI water several times and were dried at 60 °C for 24 hours.

For nanocomposite synthesis, both the materials were taken as synthesized and mixed in 1 : 1, 1 : 2 and 2 : 1 weight ratios. The mixtures were mixed in mortar pestle until a homogeneous composition was obtained. They were then kept for annealing in the programmable furnace at 450 °C for one hour and allowed to cool at room temperature. A schematic for synthesis is provided in the supporting information as Fig. S1.

2. Characterization

The crystal structure of pure $BiVO_4$, pure ZnO and ZnO-$BiVO_4$ (1 : 1) nanocomposite was determined by powder X-ray diffraction (Rigaku, D2-Phaser). The X-ray diffractograms were recorded in the range of 2θ=10 to 80° using Cu Kα radiation (λ=0.15406 nm) with a scan rate of 1°/min. The sample morphologies were studied by using transmission electron microscopy (TEM) (FEI Technai G2 200 kV). Elemental analysis of nanocomposite was confirmed by energy dispersive spectroscopy (EDAX detector in TEM). UV absorption spectra were recorded by Perkin-Elmer lambda 35 UV-Visible spectrometer having a wavelength between 200-800 nm. The photoluminescence emission spectra were obtained using HORIBA LabRAM HR Evolution at the excitation wavelength of 325 nm. The spectrum was recorded from 350-800 nm. Time-correlated single photon counting (TCSPC) using Edinburgh Instruments FLSP920 was used to collect luminescence lifetime decays. A 377 nm pulsed laser diode with a 500 kHz pulse repetition rate was used for the lifetime measurements. PL peak maximum for each sample was used to collect their PL emission decay. XPS measurements were performed using electron energy analyser (Specs GmbH, Germany, Model: PHOIBOS 150) and a non-monochromatic Al Kα X-ray source (hv=1486.61 eV) with the base pressure of $<1\times10^{-9}$ mbar.

3. Photocatalytic Study

Photocatalytic activity was determined on Methylene Blue (MB) and Rhodamine B (RhB) to test dye degradation. The sample was prepared by taking 5 mg of photocatalyst in 100 ml aqueous solution of 10 μmolar MB. The solution was ultrasonicated for two hours and further stirred for one hour under dark to remove the agglomeration and uniformly disperse the photocatalyst nano particles in the solution. Same procedure was followed to prepare the solution with RhB. Samples were put under the simulated AM 1.5 solar illumination at 100 mW/cm^2 from a xenon arc lamp in ambient atmosphere and UV-vis spectrum were recorded after interval of every 15 minutes to observe the change in the dye concentration. In this way, several readings were collected, starting from zero minute. C/C_0 curve for each sample was plotted against time, where C_0 is the initial concentration of dye at zero minute and C is the concentration of dye at various time intervals. Dye degradation efficiency was calculated using the formula [33].

$$\eta = \frac{C_0 - C}{C_0} * 100$$

4. Computational Method

Openmx package was used to perform DFT calculations within local atomic orbital (LCAO) approach [34]. For exchange-correlation function, generalized gradient approximation (GGA) proposed by Perdew-Burke-Ernzerhof (PBE) was used [35]. Soft pseudopotentials were used for Bi, Zn, O and V to describe the interaction between valence electron and ionic cores. In heterojunction, vacuum spacing of 15 Å was used between the layer of ZnO (101) and $BiVO_4$ lattice to avoid strong bond interaction between them. Therefore, PBE-D2 with van der Waals (vdw) correction was used to describe the long range interaction between them. Cut-off energy was set to 520 eV for the heterojunction and

400 eV for pristine structures. BFGS algorithm was used for geometrical optimization of 8X8X8 K-grid to reduce the system energy and forces up to 10^{-6} eV and 0.01 eV/Å, respectively. Band dispersion and density of states were calculated after geometrical optimization.

RESULTS AND DISCUSSION

1. Characterization of the ZnO-$BiVO_4$ Nanocomposite

The size and structure of synthesized $BiVO_4$, ZnO and ZnO-

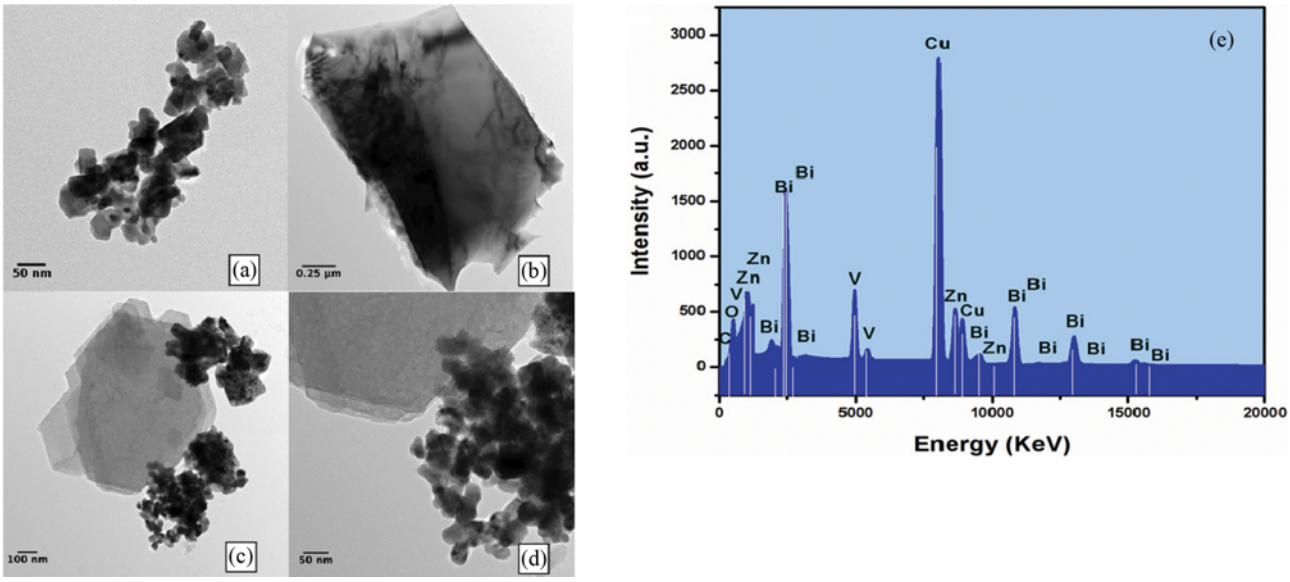

Fig. 1. TEM micrograph of (a) $BiVO_4$ nanoparticles, (b) ZnO nanosheets (c) & (d) ZnO/$BiVO_4$ (1 : 1) nanocomposite (e) EDS for ZnO-$BiVO_4$ (1 : 1) nanocomposite.

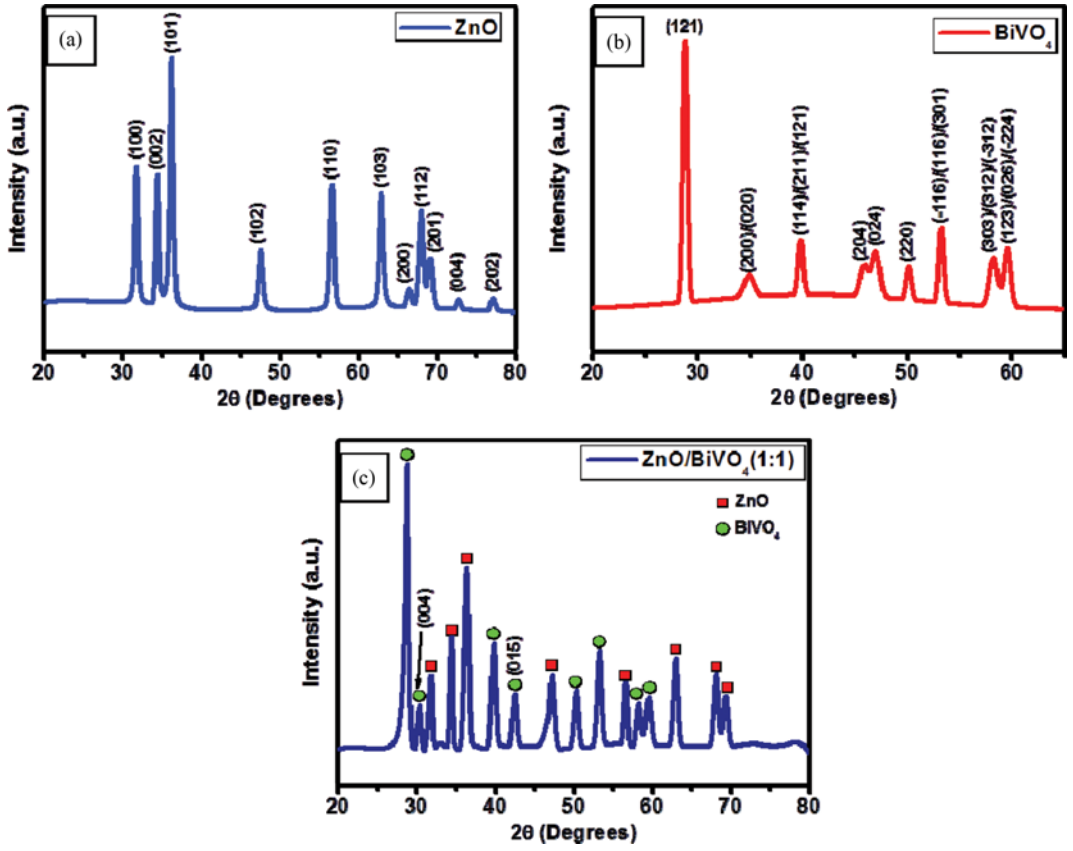

Fig. 2. XRD spectra of ZnO nanosheets (a), $BiVO_4$ nanoparticles (b) and ZnO/$BiVO_4$ nanocomposite (c).

$BiVO_4$ nanocomposite powder were investigated by transmission electron microscope. Fig. 1(a) shows the clear formation of $BiVO_4$ nanoparticles with average size of 40-100 nm. It was observed that particles were aggregated, which may be due to their self-assembly during TEM grid drying process. TEM image illustrates the overlapping ZnO nanosheets with size considerably varying from few hundred to several hundred nanometres as shown in Fig. 1(b). Nanocomposite TEM micrograph in Fig. 1(c) and (d) shows two distinct morphologies of ZnO nanosheets and $BiVO_4$ nanoparticles, also showing the incorporation of latter into former, which confirms the successful formation of ZnO-$BiVO_4$ (1 : 1) nanocomposite. TEM images showing complete attachment of $BiVO_4$ nanoparticles to ZnO nanosheets at lower magnification scale is shown in supporting information as Fig. S2.

Fig. 1(e) shows the EDS of the ZnO-$BiVO_4$ nanocomposite and confirms the presence of zinc, bismuth, vanadate and oxygen. Copper peak is due to the copper grid used in TEM sample preparation.

Fig. 2 shows the XRD patterns of $BiVO_4$, ZnO, ZnO-$BiVO_4$ (1 : 1) nanocomposite. All the peaks of ZnO and $BiVO_4$ in Fig. 2(a) and (b) are in good match with JCPDS card No. 36-1451 and 83-1699, respectively. The calculated values of lattice parameters of ZnO (a=3.25 Å, c=5.2 Å) and $BiVO_4$ (a=5.189 Å, b=5.080 Å, c=11.73 Å, γ=90.41°) were found to be consistent with the standard values, confirming the wurtzite hexagonal and monoclinic crystal structure, respectively. XRD diffractogram for ZnO-$BiVO_4$ nanocomposite, Fig. 2(c), exhibited characteristic peaks of both ZnO and $BiVO_4$. There was no change in phase of both the materials in nanocomposite, rather a change in crystallinity was observed as evidenced from the change in FWHM values. In case of ZnO nanosheet, values of FWHM for the planes (100), (002), (101) changed from 0.56, 0.46, 0.62 to 0.45, 0.34, 0.6 radian, respectively, which shows an increase in crystallite size, whereas in $BiVO_4$ FWHM values corresponding to the plane (121), (114) changed from 0.38, 0.58 to 0.64, 0.82 radian, respectively, which indicates the decrease in crystallite size.

Further, no distortion in crystal lattice of ZnO and $BiVO_4$ in composite was observed as the calculated values for a_{ZnO}, b_{ZnO} and a_{BiVO_4}, b_{BiVO_4}, c_{BiVO_4}, γ_{BiVO_4}, were in good agreement with the correspond-

Table 1. Crystal Lattice data of ZnO, $BiVO_4$ and ZnO-$BiVO_4$ (1 : 1)

Sample	a (Å)	b (Å)	c (Å)	γ (Degree)
ZnO	3.25	5.2	N.A.	N.A.
$BiVO_4$	5.189	5.080	11.73	90.41
ZnO-$BiVO_4$ (1 : 1) composite	a_{ZnO}=3.23 a_{BiVO_4}=5.19	b_{BiVO_4}=4.94	c_{ZnO}=5.194 c_{BiVO_4}=11.766	γ_{BiVO_4}=90.86

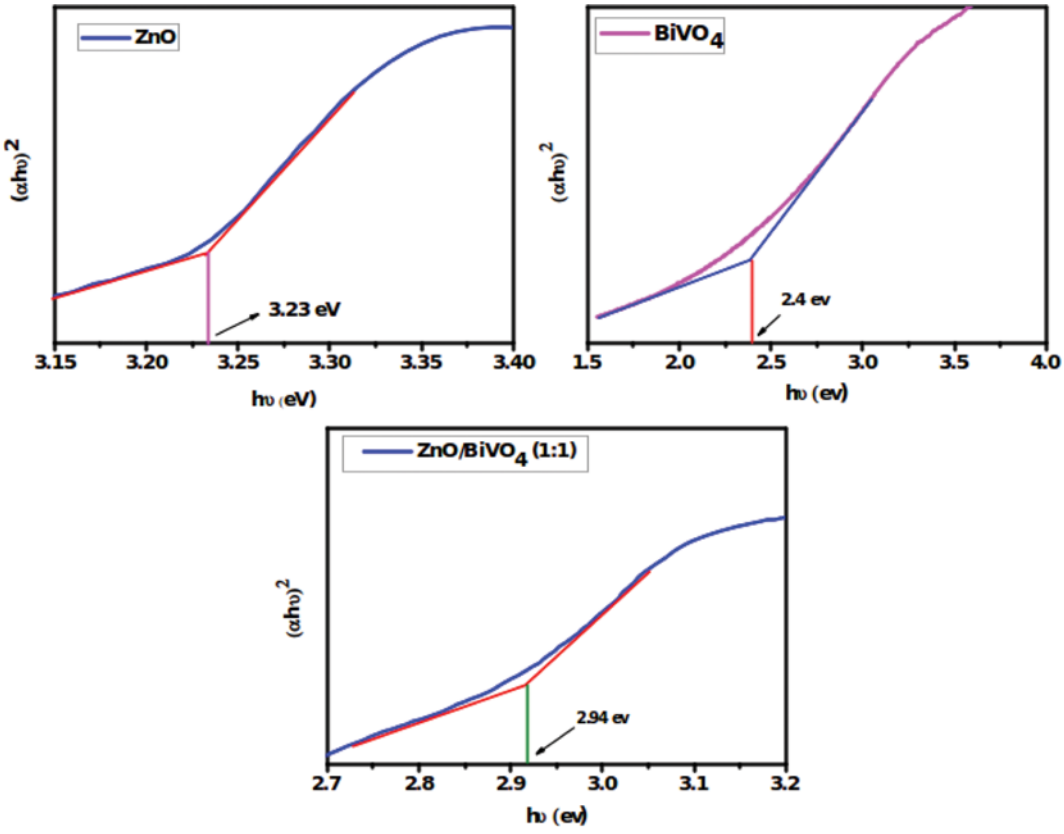

Fig. 3. Tauc's plot for ZnO nanosheets (a), $BiVO_4$ nanoparticles (b) and ZnO-$BiVO_4$ nanocomposite (c).

ing values of the pristine samples, thus indicating no phase change in the composite (Table 1). XRD pattern of composite also reveals the formation of two new planes of $BiVO_4$ at (004) and (015), respectively, which were originally not present in pristine sample.

Fig. 3(a), (b), (c) shows the Tauc's plot for ZnO, $BiVO_4$ and ZnO-$BiVO_4$ (1 : 1) nanocomposite as calculated from their respective UV emission spectra. Band gap of material was determined using Tauc's plot as obtained by plotting $(\alpha h\upsilon)^{1/n}$ versus $(h\upsilon)$, where α is the absorption coefficient of the material and n denotes the nature of transition. ZnO and $BiVO_4$ exhibits direct allowed transition for which value of $n=1/2$[33, 36]. Band gaps were observed to be 3.23 eV, 2.4 eV and 2.94 eV for ZnO, $BiVO_4$ and nanocomposite, respectively.

Fig. 4(a), (b), (c) show the room temperature PL emission spectra of pure ZnO, pure $BiVO_4$ and ZnO-$BiVO_4$ (1 : 1) nanocomposite. Near band edge UV emission peak for ZnO was recorded at 383 nm (3.23 eV) and broad green emission peak at 532 nm was observed owing to various oxygen vacancies [37] on the sample surface. $BiVO_4$ PL peak at 514 nm (2.4 eV) corresponds to near band edge emission. A shift in PL emission peak was observed in nanocomposite in comparison to pure ZnO sample, which is due to the presence of $BiVO_4$ in the sample. A strong PL emission peak was observed at 421 nm (2.94 eV) for nanocomposite, which is approximately equal to the energy difference between the valence band (VB) of $BiVO_4$ and conduction band (CB) of ZnO, which clearly indicates that maximum electron transition is taking place between these two energy bands. Thus, in nanocomposite VB of $BiVO_4$ acts as an intermediate band between VB and CB of ZnO at interface. Due to this intermediate band, the amount of energy required for electrons to jump from VB to CB of ZnO is reduced (2.94 eV), which makes nanocomposite photoactive in visible region.

PL decay curves were studied to better understand the recombination process, Fig. 4(d). Following equation was used to define the curves fitted with bi-exponential decay response:

$$y = y_0 + A_1 e^{\frac{-(x-x_0)}{t_1}} + A_2 e^{\frac{-(x-x_0)}{t_2}}$$

where y_0 is the baseline correction, t_1, t_2 are the decay constants and A_1, A_2 are the pre-exponential factors.

Following formula [38,39] was used to calculate the average decay time, τ_{avg}:

$$\tau_{avg} = \frac{\Sigma_{i=1}^{i=2} A_i t_i^2}{\Sigma_{i=1}^{i=2} A_i t_i}$$

The average lifetime, using above equation, for ZnO-$BiVO_4$ (1 : 1), ZnO-$BiVO_4$ (1 : 2), ZnO-$BiVO_4$ (2 : 1) was calculated to be 37, 27 and 25 ns, respectively. ZnO-$BiVO_4$ (1 : 1) has an increased lifetime compared to ZnO-$BiVO_4$ (1 : 2), ZnO-$BiVO_4$ (2 : 1). Several factors affect the lifetime of charge carriers such as carrier trapping, band structure, and mobility of charge carriers. It was stated

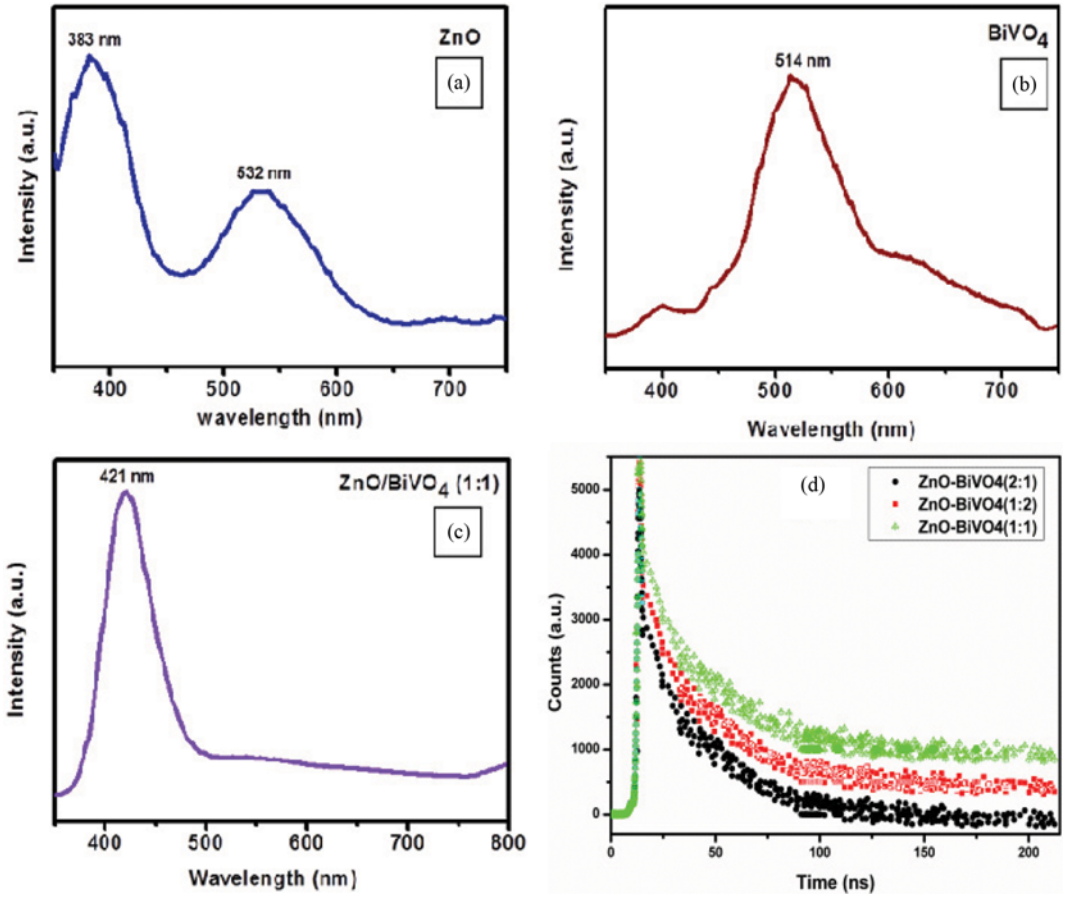

Fig. 4. Photoluminescence for ZnO nanosheets (a), $BiVO_4$ nanoparticles (b), ZnO-$BiVO_4$ nanocomposite (c) and luminescence decay study (d).

by Baiju et al. that the longer lifetime is also the result of interface formation between different materials in the interface [40]. So the above data clearly indicates the best interface formation in ZnO-$BiVO_4$ (1 : 1) in comparison to ZnO-$BiVO_4$ (1 : 2), ZnO-$BiVO_4$ (2 : 1).

The VB and CB band edge positions were calculated using Mulliken electronegativity theory given by formula:

$$E_{VB}=X-E_e+0.5E_g$$
$$E_{CB}=E_{VB}-E_g$$

where E_{VB} is the valence band edge potential, E_{CB} is the conduction band edge potential, X is the absolute electronegativity, E_e is the energy of free electrons which is ~4.5 eV on the hydrogen scale and E_g is the band gap energy of the semiconductor. Value of X for ZnO and $BiVO_4$ is 5.95 and 6.04 eV, respectively [41,42]. The E_{CB} of ZnO and $BiVO_4$ are calculated and found to be −0.16 eV and 0.34 eV, respectively. The E_{VB} of ZnO and $BiVO_4$ are estimated to be 3.06 and 2.74 eV, respectively. The energy gap between CB of ZnO and VB of $BiVO_4$ almost equals the band gap of the material (~2.9 eV), thus showing that maximum charge transitions are taking place between the two bands as also confirmed from UV and PL studies.

The XPS was obtained to analyze the surface chemical composition and oxidation state of ZnO-$BiVO_4$ nanocomposite and to further study the interaction of ZnO with the $BiVO_4$ support. XPS spectra of O 1s and Zn 2p for pure ZnO and ZnO-$BiVO_4$ heterojunction, as well as the V 2p and Bi 4f spectra for the pure $BiVO_4$ and heterojunction are shown in Fig. 5. The binding energy values of Zn 2p1/2 and Zn 2p3/2 were observed at 1,044.49 and 1,021.09 eV (Fig. 5(a)), respectively, which can be accredited to the Zn^{2+} ions of the ZnO after comparing peak positions with the Handbook of X-ray Photoelectron Spectroscopy [43]. However, the binding energies of Zn 2p1/2 and Zn 2p3/2 for ZnO-$BiVO_4$ heterojunction were 1,044.8 and 1,021.6 eV, respectively, which are higher than those for pure ZnO. The XPS peaks for O 1s (530.19 and 529.79 eV) endured the same binding energies, as shown in Fig. 5(b). Such chemically shifted peaks of Zn 2p in the heterojunction can be ascribed to the Zn interaction with Bi and V. Furthermore, the emergence of new Bi 4f peak at 157.63 eV (Fig. 5(d)) and the red shift of V2p peak from 519.59 to 516.27 eV (Fig. 5(c)) in composite indeed reveals that the $BiVO_4$ structure has undergone changes after interaction with ZnO to construct a heterojunction, which confirms the presence of interface between ZnO and $BiVO_4$.

2. DFT Computations on the Interaction of Heterojunction

To investigate the interaction between ZnO and $BiVO_4$ at the heterojunction, DFT calculations were performed on the theoretical model of the interface. Based on XRD results, ZnO slab corresponding to (101) plane was considered for calculations. We first investigated the lattice structure of pristine ZnO(101), $BiVO_4$ and ZnO(101)-$BiVO_4$ heterojunction. Negligible change in atomic coordinates of ZnO(101) and $BiVO_4$ was observed after geometrical optimization. In ZnO(101)-$BiVO_4$ heterojunction, calculated vacuum spacing between ZnO(101) and $BiVO_4$ after geometrical optimization was 2.36 Å (Fig. 6). It is widely known that close contact between different materials in composite is advantageous for charge transfer and separation.

To investigate the enhanced photo-catalytic activity of the ZnO (101)-$BiVO_4$ heterojunction, we calculated its band structure. Band

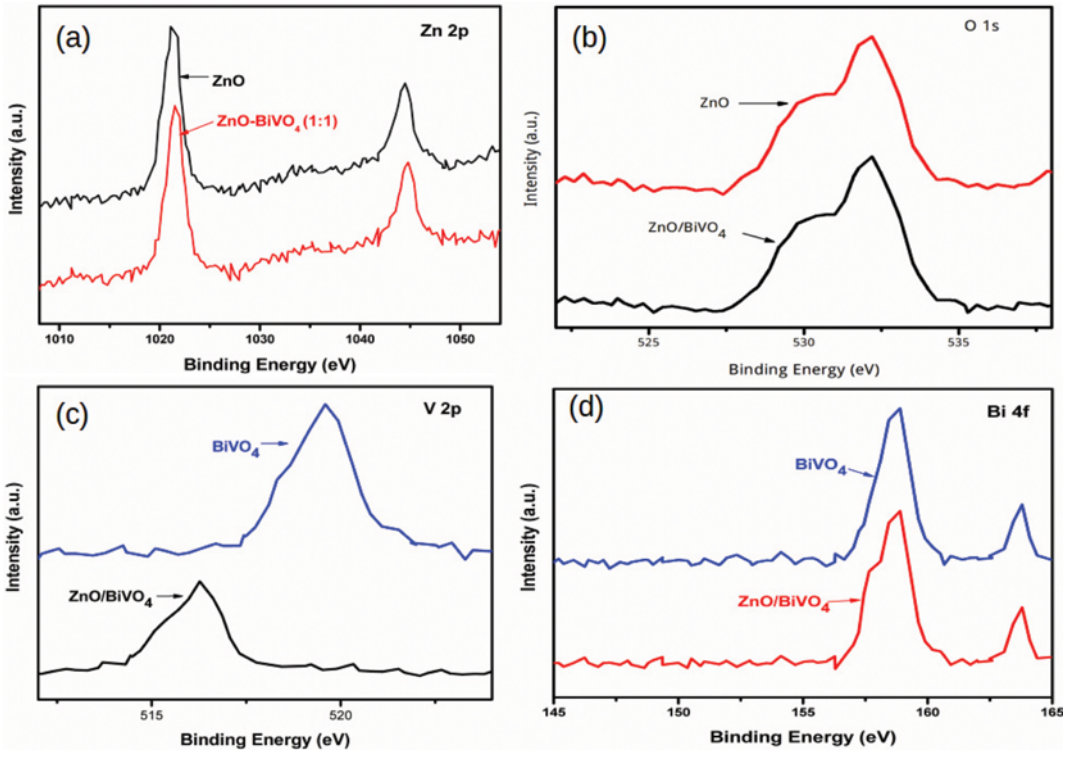

Fig. 5. XPS spectra for: (a) Zn 2p peak of pure ZnO and ZnO-$BiVO_4$ heterojunction; (b) O1s peak of pure ZnO and ZnO-$BiVO_4$ heterojunction; (c) V 2p peak of pure $BiVO_4$ and ZnO-$BiVO_4$ heterojunction; (d) Bi 4fpeak of pure $BiVO_4$ and ZnO-$BiVO_4$ heterojunction.

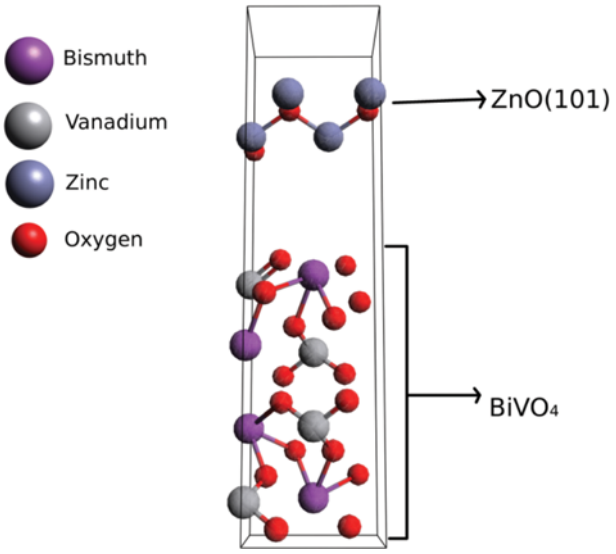

Fig. 6. ZnO(101)-$BiVO_4$ heterojunction optimized geometrical structure.

structures of ZnO(101) and $BiVO_4$ were also calculated for comparison. Band structures are shown in Fig. 7. ZnO(101) was direct band bap semiconductor with 0.91 eV as calculated band gap as shown in Fig. 7(a), which is in good agreement with previously calculated results [44,45]. $BiVO_4$ band structure indicated indirect band gap of 2.16 eV with valence band maximum at L-M and conduction band minimum at L as shown in Fig. 7(b). Calculated band gap of $BiVO_4$ is also in good agreement with previously calculated results [46]. ZnO(101)-$BiVO_4$ heterojunction had indirect band gap of 1.8 eV with valence band maximum at Z and conduction band minimum at G in Fig. 7(c). The calculated values of band gaps are not reliable [47] due to commonly known shortcoming of DFT.

Further, total density of states (TDOS) and project density of states (PDOS) were calculated as shown in Fig. 8(a), (b) and (c). Below Fermi level at 0 eV, in ZnO(101) valence band was formed by Zn s, Zn p and O p orbitals. Valence band in $BiVO_4$ mainly consisted of Bi s and O p orbital. Above the Fermi level, conduction band of ZnO(101) was formed by Zn s and in $BiVO_4$ it was mainly formed by Bi p, O p and V d orbitals. In ZnO(101)-$BiVO_4$ heterojunction, valence band maximum was mainly occupied by Bi s orbital and conduction band minimum was occupied by Zn s orbital which indicates the maximum electron transition from $BiVO_4$ valence band to ZnO conduction band in ZnO-$BiVO_4$ composite as also confirmed by photoluminescence study.

3. Photocatalytic Activity of the Heterojunctions

Fig. 9(a) shows the C/C_o curves for ZnO, $BiVO_4$, ZnO-$BiVO_4$ (1 : 1), ZnO-$BiVO_4$ (1 : 2) and ZnO-$BiVO_4$ (2 : 1) samples for MB dye solution. As indicated from the curves, the photocatalytic dye degradation efficiencies are (0%, 6.1%, 11.1%, 15.8%, 20%) for MB dye (without Photocatalyst), (0%, 17.4%, 27.6%, 39.9%, 45.2%) for $BiVO_4$, (0%, 23.6%, 37.4%, 48.7%, 57.3%) for ZnO, (0%, 25.1%, 45.8%, 59.9%, 77.8%) for ZnO-$BiVO_4$ (2 : 1), (0%, 30.7%, 48.4%, 74.6%, 86%) for ZnO-$BiVO_4$ (1 : 1) and (0%, 18.1%, 28.1%, 38.2%, 46.4%) for ZnO-$BiVO_4$ (1 : 2) at the intervals of 0, 15, 30, 45, 60 minutes, respectively. The above results indicate that ZnO-$BiVO_4$ (1 : 1) exhibits the highest dye degradation efficiency of 77.8% in 60 minutes.

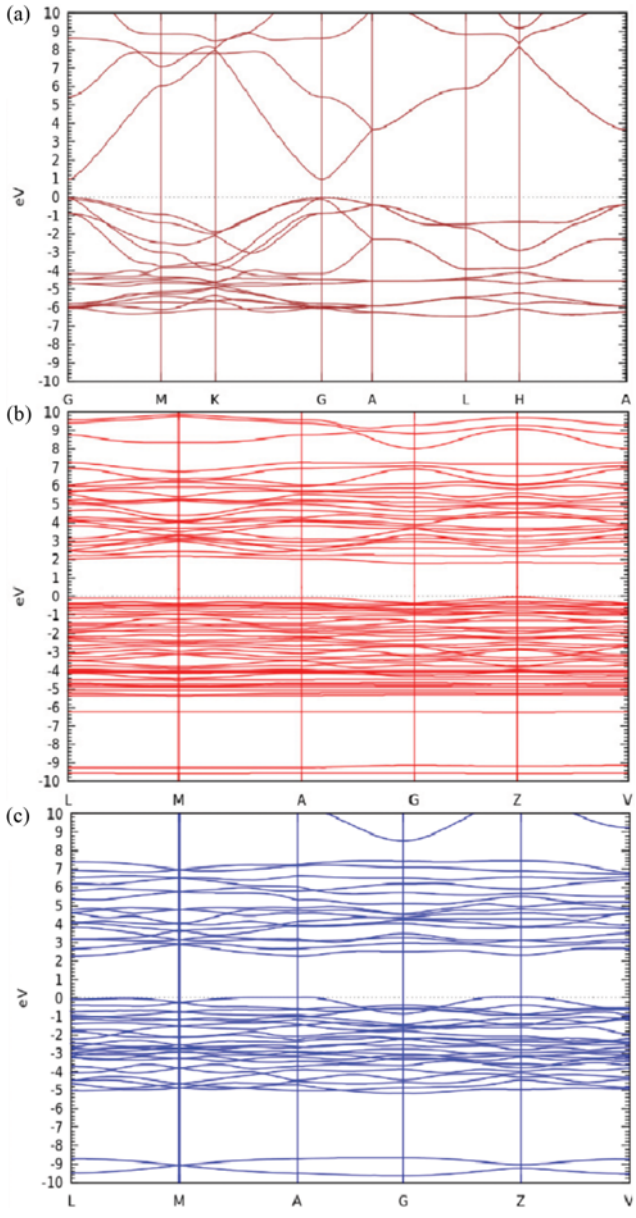

Fig. 7. Calculated band structures of (a) ZnO, (b) $BiVO_4$, and (c) ZnO-$BiVO_4$ heterojunction.

Photodegradation follows pseudo first-order kinetics and is given by:

$$C_t = C_0 e^{-kt}$$

or

$$-\ln\left(\frac{C_t}{C_0}\right) = Kt$$

where C_0 is the initial concentration, C_t is the concentration after time t, and k is the rate constant of pseudo first-order reaction [48,49].

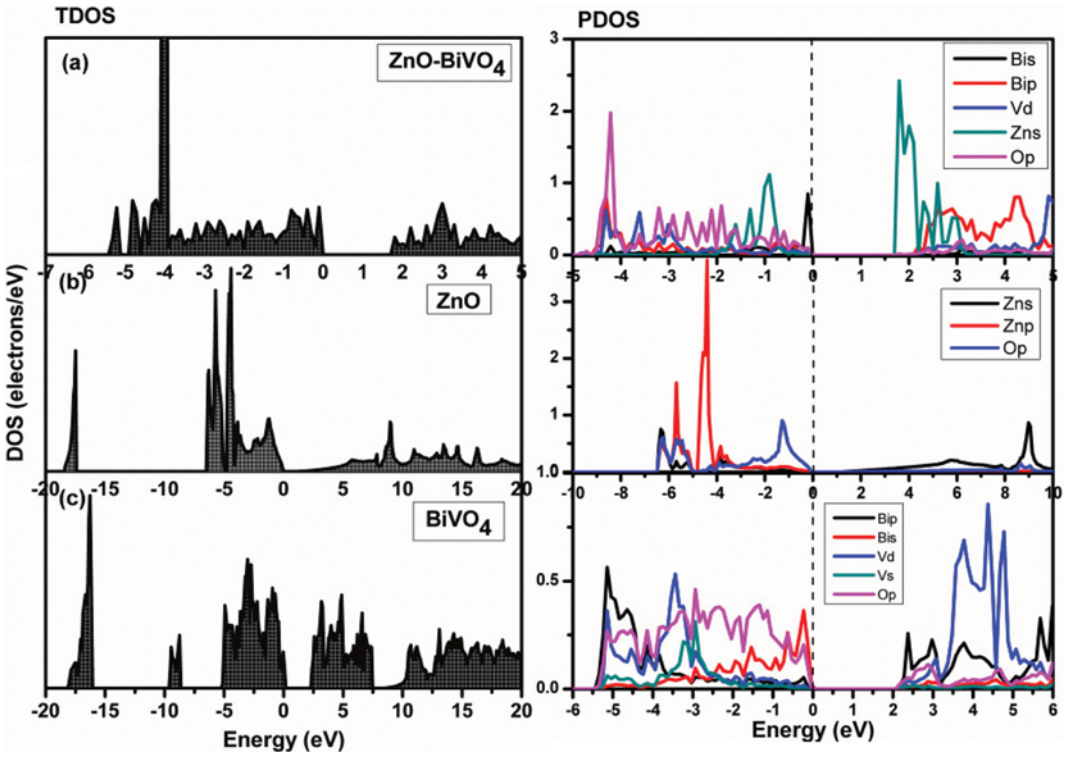

Fig. 8. Calculated TDOS and PDOS of (a) ZnO-$BiVO_4$ heterojunction (b) ZnO (c) $BiVO_4$ heterojunction. The vertical line is Fermi level.

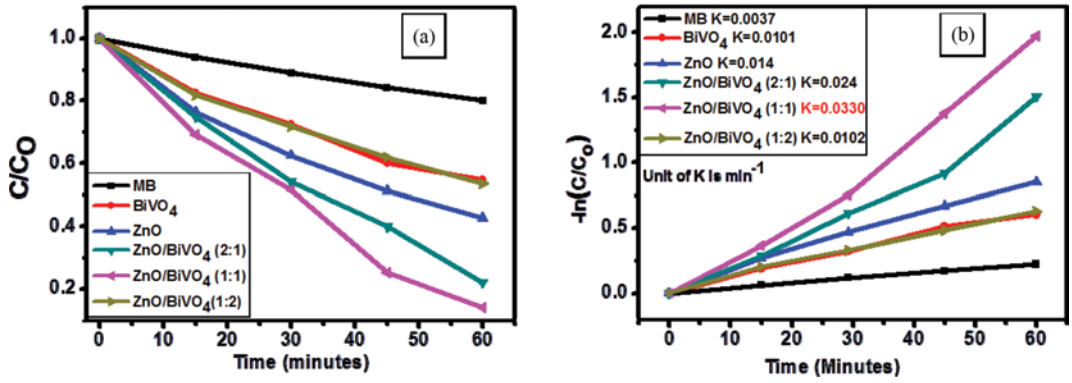

Fig. 9. C/Co curves for ZnO, $BiVO_4$, ZnO-$BiVO_4$ (1 : 1), ZnO-$BiVO_4$ (1 : 2) and ZnO-$BiVO_4$ (2 : 1) samples for MB dye solution (a) and first order rate kinetics of MB dye degradation for various samples (b).

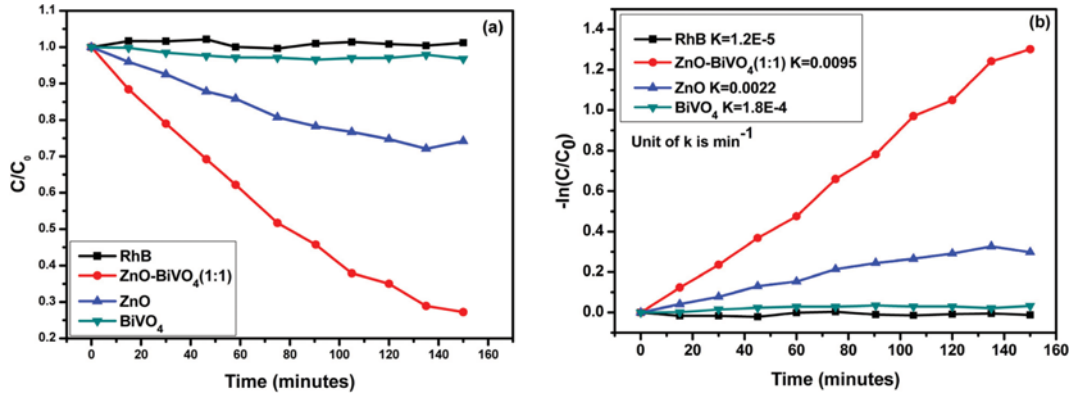

Fig. 10. C/C_0 curve (a) and First order rate kinetics (b) of ZnO-$BiVO_4$ (1 : 1) sample for RhB dye degradation.

Fig. 9(b) shows the plot between $-\ln(C_0/C_t)$ and time (t) for various samples. The values for pseudo first-order reaction rate constants as given by the slope of the curves are k=0.0037 min^{-1} for MB (without photocatalyst), 0.0101 min^{-1} for $BiVO_4$, 0.014 min^{-1} for ZnO, 0.024 min^{-1} for ZnO/$BiVO_4$ (2 : 1), 0.0330 min^{-1} ZnO/$BiVO_4$ (1 : 1) and 0.0102 min^{-1} for ZnO/$BiVO_4$ (1 : 2). Thus, degradation rate of MB by ZnO/$BiVO_4$ (1 : 1) is highest and is approximately 2.5 times faster as compared to pure ZnO.

Dye degradation efficiency of ZnO-$BiVO_4$ (1 : 1) sample for RhB dye is 72.7% in 150 minutes as shown in Fig. 10(a). Rate constant of pseudo first-order kinetics is 0.0095 min^{-1}, which is 4.3 times higher than ZnO as shown in Fig. 10(b). From above results it is clear that ZnO/$BiVO_4$ exhibits higher degradation efficiency on MB in comparison to RhB. The probable reason for this difference is discussed in supporting information as Fig. S3.

Photostability of ZnO-$BiVO_4$ (1 : 1) nanocomposite was also investigated as shown in Fig. 11. No significant loss in activity was observed up to five cycles and catalyst exhibited a highly stable photocatalytic performance towards MB degradation.

4. Proposed Mechanism of Photocatalysis in ZnO-$BiVO_4$ Nanocomposite

A possible mechanism for improved photo catalytic activity of ZnO-$BiVO_4$ nano composite is presented in this section. It is well known that in ZnO, surface defects are common and various physical processes such as grinding and mechanical-milling generates more amount of such defects in the material that contribute in altering its surface chemistry, optical and electronic properties [50-52]. To verify this in our case too, we conducted a PL study of pure ZnO, with and without mechanical milling process, as shown in Fig. S4. Clearly, ZnO after milling contains an overall increase in various surface defects as seen from the origin of multiple peaks in the defect band in PL Therefore, when this ZnO is combined to a different material to form a composite, it establishes a bond of interaction with the latter due to the presence of a large number of defects on its surface, which proves to be a source of chemical interaction between the two [53,54]. Similarly, in our case when ZnO is coupled to $BiVO_4$ through the process of milling followed by high temperature annealing, these defects act as active high energy sites favorable for adsorption of the $BiVO_4$ on ZnO surface through weak chemical bond. This existence of chemical interaction between the two materials was also revealed through the XPS spectra of composite, which shows a shift in the binding energies of Zn, Bi and V as compared to energies of their pure counterparts. Moreover, in the PL study of the composite we observed that ZnO near band edge and defect peaks were suppressed and only a major peak at 421 nm was present, which corresponds to energy of 2.94 eV and could only be formed due to the major electron transition from VB of $BiVO_4$ and CB of ZnO supported by estimated band edge potentials of both the materials. Nonappearance of defect PL peaks of ZnO in composite is attributed to the chemical adsorption of $BiVO_4$ on the defect sites of ZnO, so the presence of $BiVO_4$ in ZnO highly suppresses the defect inter band electron transition in ZnO and VB of $BiVO_4$ itself is acting as inter band for electron transition to take place. Such intermediate band formation in composites was reported earlier [55,56]. Also, in DFT calculations the ZnO sheet structure considered for calculations have terminated zinc and oxygen bonds at the edges. Band structure and density of states calculations performed considering terminated bond-ZnO sheet also confirmed the electron transition from VB of $BiVO_4$ to CB of ZnO.

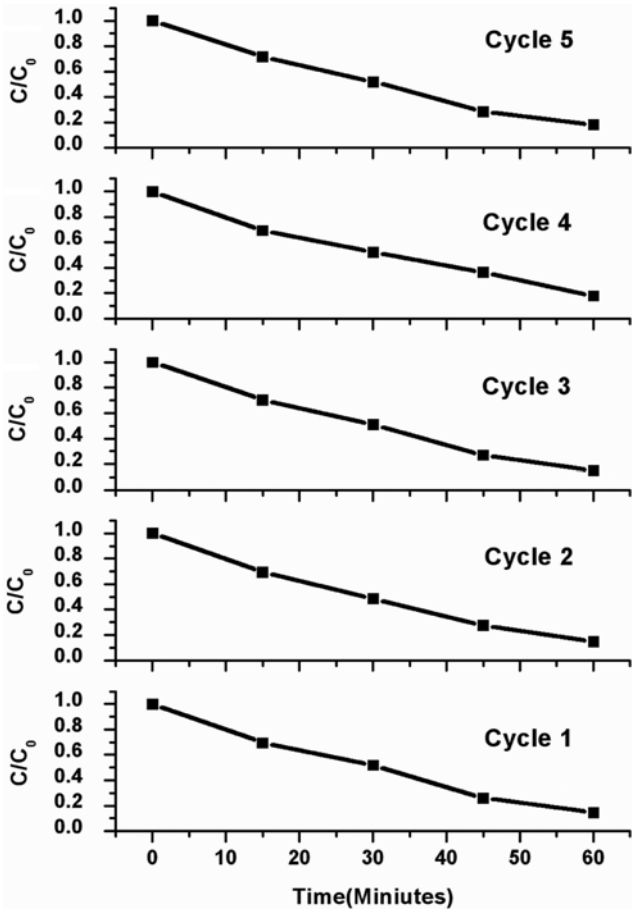

Fig. 11. Repeatability test for ZnO-$BiVO_4$ (1 : 1) nanocomposite using MB dye.

So, presence of this intermediate band reduces the amount of energy to 2.94 eV from 3.23 eV (band gap of ZnO) required for electron transition to the conduction band of ZnO, thus making nanocomposite photoactive in visible region of solar spectrum. In photocatalytic process, when light falls on nanocomposite surface, an electron transition takes place between newly formed intermediate band and CB of ZnO. These electrons in CB of ZnO reduce the adsorbed oxygen to form O_2^- super oxides [10,57,58].

These reactive ions undergo reaction with water to form hydrogen peroxide (H_2O_2). Electron–hole pair in intermediate band and CB of ZnO has enough electrochemical potential to redox water to form H^+ and hydroxyl ions (OH^-). These OH^- ions produced lose their electron to holes in intermediate band (VB of $BiVO_4$) to form •OH radicals [47,48]. These reactive species (O_2^-, H_2O_2, •OH) further react with the dye present in the solution and result in dye degradation.

$$ZnO/BiVO_4 + hv \rightarrow e^- + h^+$$
$$e^- + O_2 \rightarrow O_2^-$$
$$O_2^- + 2H_2O \rightarrow 2H_2O_2$$

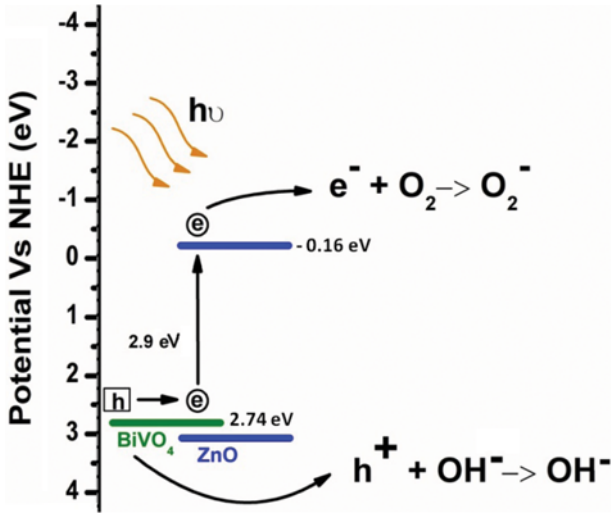

Fig. 12. Mechanism of action of nanocomposite photocatalyst.

$h^+ + OH^- \rightarrow \bullet OH$

$Dye + O_2^- + H_2O_2 + \bullet OH \rightarrow$ Dye Degradation

CONCLUSION

We prepared ZnO-$BiVO_4$ hetero-structured photocatalyst. The XPS results indicated that ZnO and $BiVO_4$ were in close contact and formed an interface at heterojunction. The electronic structure of the ZnO-$BiVO_4$ nanocomposite was investigated through DFT calculations. The as-prepared heterostructured photocatalysts showed 2.5 and 3.5 times better visible-light driven photocatalytic activity for degradation of MB than pure ZnO and $BiVO_4$, respectively. Bi s orbital of $BiVO_4$ in ZnO-$BiVO_4$ forms the intermediate band in ZnO and reduces the band gap of the material, which then requires less energy to become photoactive. The charge transfer process, upon irradiation, takes place from VB of $BiVO_4$ acting as intermediate band to the CB of ZnO. This makes the material sensitive towards the visible region of solar spectrum and thus shows high photocatalytic activity. Further, low recombination rate exhibited by ZnO-$BiVO_4$ (1 : 1) adds to its superior photoactivity and remarkable results. Our results provide insight into understanding the mechanism of heterojunction on photocatalytic activity, which will help in designing new heterojunctions for photocatalytic reactions for dye degradation and water splitting applications.

ACKNOWLEDGEMENTS

Authors are highly grateful to the Chancellor Dr S. J. Chopra, University of Petroleum & Energy Studies Dehradun. Authors also feel a deep sense of gratitude to the Nano Research Facility (NRF), Indian Institute of Technology, Delhi-110016, for providing characterization facility.

SUPPORTING INFORMATION

Additional information as noted in the text. This information is available via the Internet at http://www.springer.com/chemistry/journal/11814.

REFERENCES

1. M. N. Chong, B. Jin, C. W. K. Chow and C. Saint, *Water Res.*, **44**, 2997 (2010).
2. S. Dong, J. Feng, M. Fan, Y. Pi, L. Hu, X. Han, M. Liu, J. Sun and J. Sun, *RSC Adv.*, **5**, 14610 (2015).
3. P. Venkata, L. Reddy, K. H. Kim and Y. H. Kim, *Asian J. Atmos. Environ.*, **5**, 181 (2011).
4. J. Zhao and X. Yang, *Build. Environ.*, **38**, 645 (2003).
5. E. Boonen and A. Beeldens, *Coatings*, **4**, 553 (2014).
6. D. Chatterjee and S. Dasgupta, *J. Photochem. Photobiol. C Photochem. Rev.*, **6**, 186 (2005).
7. J. Zhao, C. Chen and W. Ma, *Top. Catal.*, **35**, 269 (2005).
8. R. Michal, S. Sfaelou and P. Lianos, *Molecules*, **19**, 19732 (2014).
9. M. De Oliveira Melo and L. A. Silva, *J. Braz. Chem. Soc.*, **22**, 1399 (2011).
10. A. Ajmal, I. Majeed, R. N. Malik, H. Idriss and M. A. Nadeem, *RSC Adv.*, **4**, 37003 (2014).
11. K. Maeda, *J. Photochem. Photobiol. C Photochem. Rev.*, **12**, 237 (2011).
12. S. J. A. Moniz, S. A. Shevlin, D. J. Martin, Z.-X. Guo and J. Tang, *Energy Environ. Sci.*, **8**, 731 (2015).
13. K. Hashimoto, H. Irie and A. Fujishima, *Jpn. J. Appl. Phys.*, **44**, 8269 (2005).
14. J. Schneider, M. Matsuoka, M. Takeuchi, J. Zhang, Y. Horiuchi, M. Anpo and D. W. Bahnemann, *Chem. Rev.*, **114**, 9919 (2014).
15. C. Siriwong, N. Wetchakun, B. Inceesungvorn, D. Channei, T. Samerjai and S. Phanichphant, *Prog. Cryst. Growth Charact. Mater.*, **58**, 145 (2012).
16. H. Chen and L. Wang, *Beilstein J. Nanotechnol.*, **5**, 696 (2014).
17. M. M. Khan, S. F. Adil and A. Al-Mayouf, *J. Saudi Chem. Soc.*, **19**, 462 (2015).
18. R. Ullah and J. Dutta, *J. Hazard. Mater.*, **156**, 194 (2008).
19. C. Mondal, J. Pal, M. Ganguly, A. K. Sinha, J. Jana and T. Pal, *New J. Chem.*, **38**, 2999 (2014).
20. C. Yu, K. Yang, Y. Xie, Q. Fan, J. C. Yu, Q. Shu and C. Wang, *Nanoscale*, **5**, 2142 (2013).
21. R. Saravanan, M. M. Khan, V. K. Gupta, E. Mosquera, F. Gracia, V. Narayanan and A. Stephen, *RSC Adv.*, **5**, 34645 (2015).
22. J. P. Dhal, B. G. Mishra and G. Hota, *RSC Adv.*, **5**, 58072 (2015).
23. B. Panigrahy and D. D. Sarma, *RSC Adv.*, **5**, 8918 (2015).
24. M. Gratzel, Nat. (London, U. K.) **414**, 338 (2001).
25. M. Han, X. Chen, T. Sun, O. K. Tan and M. S. Tse, *CrystEngComm*, **13**, 6674 (2011).
26. Y. Park, K. J. McDonald and K.-S. Choi, *Chem. Soc. Rev.*, **42**, 2321 (2013).
27. Michael G. Walter, Emily L. Warren, James R. McKone, Shannon W. Boettcher, Qixi Mi, Elizabeth A. Santori and Nathan S. Lewis, *Chem. Rev.*, **110**, 6446 (2010).
28. S. Balachandran, N. Prakash, K. Thirumalai, M. Muruganandham, M. Sillanp and M. Swaminathan, *Ind. Eng. Chem. Res.*, **53**, 8346 (2014).
29. X. Fu, M. Xie, P. Luan and L. Jing, *ACS Appl. Mater. Interfaces*, **6**,

18550 (2014).
30. S. J. A. Moniz, J. Zhu and J. Tang, *Adv. Energy Mater.*, **4**, 1 (2014).
31. C. Yang, M. Qin, Y. Wang, D. Wan, F. Huang and J. Lin, *Sci. Rep.*, **3**, 1286 (2013).
32. D. Ke, T. Peng, L. Ma, P. Cai and K. Dai, *Inorg. Chem.*, **48**, 4685 (2009).
33. T. Bhuyan, M. Khanuja, R. Sharma, S. Patel, M. R. Reddy, S. Anand and A. Varma, *J. Nanoparticle Res.*, **17**, 288 (2015).
34. H. Lin, J. Cao, B. Luo, B. Xu and S. Chen, *Chinese Sci. Bull.*, **57**, 2901 (2012).
35. J. P. Perdew, K. Burke and M. Ernzerhof, *Phys. Rev. Lett.*, **77**, 3865 (1996).
36. Y. Liu, H. Dai, J. Deng, L. Zhang and C. T. Au, *Nanoscale*, **4**, 2317 (2012).
37. M. K. Kavitha, P. Gopinath and H. John, *Phys. Chem. Chem. Phys.*, **17**, 14647 (2015).
38. K. Das, S. N. Sharma, M. Kumar and S. K. De, *J. Phys. Chem. C*, **113**, 14783 (2009).
39. S. Paul and A. Choudhury, *Appl. Nanosci.*, **4**, 839 (2013).
40. K. V. Baiju, A. Zachariah, S. Shukla, S. Biju, M. L. P. Reddy and K. G. K. Warrier, *Catal. Lett.*, **130**, 130 (2009).
41. P. Y. Kuang, J. R. Ran, Z. Q. Liu, H. J. Wang, N. Li, Y. Z. Su, Y. G. Jin and S. Z. Qiao, *Chem. - A Eur. J.*, **21**, 15360 (2015).
42. J. Zhang, F. Ren, M. Deng and Y. Wang, *Phys. Chem. Chem. Phys.*, **17**, 10218 (2015).
43. X. Chang, J. Huang, Q. Tan, M. Wang, G. Ji, S. Deng and G. Yu, *Catal. Commun.*, **10**, 1957 (2009).
44. L. Li, W. Wang, H. Liu, X. Liu, Q. Song and S. Ren, *J. Phys. Chem. C*, **113**, 8460 (2009).
45. A. A. Mohamad, M. S. Hassan, M. K. Yaakob, M. F. M. Taib, F. W. Badrudin, O. H. Hassan and M. Z. A. Yahya, *J. King Saud Univ. - Eng. Sci.*, dx.doi.org/10.1016/j.jksues.2015.08.002.
46. Z. Zhao, Z. Li and Z. Zou, *Phys. Chem. Chem. Phys.*, **13**, 4746 (2011).
47. R. W. Godby, M. Schlüter and L. J. Sham. *Phys. Rev. B*, **37**, 10159 (1988).
48. R. Mohan, K. Krishnamoorthy and S. J. Kim, *Chem. Phys. Lett.*, **83**, 539 (2012).
49. R. Mohan, K. Krishnamoorthy and S.-J. Kim, *Solid State Commun.*, **152**, 375 (2012).
50. T. Phan, Y. D. Zhang, D. S. Yang, N. X. Nghia, T. D. Thanh and S. C. Yu, *Appl. Phys. Lett.*, **102**, 072408 (2013).
51. S. Dutta, S. Chattopadhyay, M. Sutradhar, A. Sarkar, M. Chakrabarti, D. Sanyal and D. Jana, *J. Phys. Condens. Matter*, **19**, 236218 (2007).
52. X. Zhang, J. Qin, Y. Xue, P. Yu, B. Zhang, L. Wang and R. Liu, *Sci. Rep.*, **1**, 4:4596 (2014).
53. K. Laxman, T. Bora, S. H. Al-Harthi and J. Dutta, *J. Nanomater.* 2014, Article ID 919163, 1 (2014), dx.doi.org/10.1155/2014/919163.
54. S. Danwittayakul, K. Lakshman, S. Al-Harthi and J. Dutta, *Appl. Catal. A Gen.*, **471**, 63 (2014).
55. S. Divya, V. P. N. Nampoori, P. Radhakrishnan and A. Mujeeb, *Appl. Phys. A Mater. Sci. Process.*, **114**, 315 (2014).
56. S. G. Lu, Y. J. Yu, C. L. Mak, K. H. Wong, L. Y. Zhang and X. Yao, *Microelectronic Engineering*, **66**, 171 (2003).
57. M. Basu, N. Garg and A. K. Ganguli, *J. Mater. Chem. A*, **2**, 7517 (2014).
58. S. Ma, J. Xue, Y. Zhou and Z. Zhang, *J. Mater. Chem. A*, **2**, 7272 (2014).